HHS Public Access

Author manuscript

J Magn Reson Imaging. Author manuscript; available in PMC 2017 September 01.

Published in final edited form as:

J Magn Reson Imaging. 2016 September ; 44(3): 653–664. doi:10.1002/jmri.25210.

High Slew-Rate Head-Only Gradient for Improving Distortion in Echo Planar Imaging: Preliminary Experience

Ek T. Tan, Ph.D.[1], **Seung-Kyun Lee, Ph.D.**[3], **Paul T. Weavers, Ph.D.**[2], **Dominic Graziani, Ph.D.**[1], **Joseph E. Piel, B.S.**[1], **Yunhong Shu, PhD.**[2], **John Huston III, M.D.**[2], **Matt A. Bernstein, Ph.D.**[2], and **Thomas K.F. Foo, Ph.D.**[1]

[1]GE Global Research, Niskayuna, NY, USA

[2]Department of Radiology, Mayo Clinic, Rochester, MN, USA

[3]CNIR, IBS and Department of Biomedical Engineering Sungkyunkwan University, Suwon, South Korea

Abstract

Purpose—To investigate the effects on echo planar imaging (EPI) distortion of using high gradient slew rates (SR) of up to 700 T/m/s for *in-vivo* human brain imaging, with a dedicated, head-only gradient coil.

Materials and Methods—Simulation studies were first performed to determine the expected echo spacing and distortion reduction in EPI. A head gradient of 42-cm inner diameter and with asymmetric transverse coils was then installed in a whole-body, conventional 3T MRI system. Human subject imaging was performed on five subjects to determine the effects of EPI on echo spacing and signal dropout at various gradient slew rates. The feasibility of whole-brain imaging at 1.5 mm-isotropic spatial resolution was demonstrated with gradient-echo and spin-echo diffusion-weighted EPI.

Results—As compared to a whole-body gradient coil, the EPI echo spacing in the head-only gradient coil was reduced by 48%. Simulation and *in vivo* results, respectively, showed up to 25-26% and 19% improvement in signal dropout. Whole-brain imaging with EPI at 1.5 mm spatial resolution provided good whole-brain coverage, spatial linearity, and low spatial distortion effects.

Conclusion—Our results of human brain imaging with EPI using the compact head gradient coil at slew rates higher than in conventional whole-body MR systems demonstrate substantially improved image distortion, and point to a potential for benefits to non-EPI pulse sequences.

Keywords

Echo planar imaging; EPI; head-only gradient coil; slew rate; image distortion

Correspondence: Ek T. Tan, Ph.D., Diagnostics, Imaging, and Biomedical Technologies, GE Global Research, One Research Circle, Niskayuna, NY 12309, USA, Phone: 518-387-7075, Fax: 518-387-6923, ek.tan@ge.com.

INTRODUCTION

Echo planar imaging (EPI) (1), in particular single-shot two-dimensional (2D) EPI, is the most widely used readout in clinical MRI for fast imaging applications like diffusion-weighted imaging (DWI) and functional MRI. EPI allows acquisition of a 2D-plane in less than 100 ms, which mitigates motion artifacts, and obviates the need for gated acquisitions. EPI also provides rapid, 2D multi-slice acquisition that enables whole-brain DWI and functional MRI to be acquired in clinically-feasible scan times. A key enabler of using EPI in clinical MRI has been the availability of high-voltage gradient drivers (2) and the design of gradient coils that can sustain the higher applied voltage, which allow for high gradient slew rates on the order of 200 T/m/s to be routinely used in modern, conventional, whole-body MRI scanners.

The primary disadvantage of single-shot 2D EPI is severe image distortion due to spatial variation of magnetic susceptibility and the main magnetic field B_0 (3, 4). While 2D EPI traverses 2D k-space rapidly, phase accumulation during the finite echo spacing (ESP) between consecutive readouts makes EPI highly sensitive to B_0 inhomogeneity (5). This results in nonlinear spatial distortions and also non-uniform signal intensity variations such as signal 'bunching' and 'dropout' primarily along the phase-encoded (i.e., blipped) direction.

A simple strategy for reducing image distortion is to use multi-shot EPI (6) rather than single-shot EPI, albeit at the cost of increased acquisition time and increased sensitivity to patient motion between shots. Another strategy is to acquire B_0 field maps for EPI distortion correction, using either a separate acquisition (3, 7, 8) or reversed-polarity EPI readout (9-11). Even with the additional post-processing required, EPI correction is not effective in areas of high susceptibility variation where the signal loss due to dephasing is irrecoverable. Improved B_0 shimming procedures (12, 13) and shimming hardware (14, 15) have been attempted to compensate for nonlinear B_0 variation, but they have limited degrees of freedom in homogenizing B_0 in the presence of rapid spatial variation of susceptibility.

The extent of EPI distortion is proportional to its echo spacing (ESP). However, ESP is difficult to reduce in whole-body MRI systems because peripheral nerve stimulation (PNS) limits the maximum permissible slew rate to a value typically less than or equal to 200 T/m/s, and this value is further reduced at increased gradient amplitudes. Moreover, the gradient power supply limits the gradient performance; currently the highest available whole-body gradient performance of a clinical system is 80 mT/m and 200 T/m/s per-axis (using 2MVA of peak power), with 40-50 mT/m and 200 T/m/s typical for a modern whole-body gradient system (using 1MVA of peak power).

One way to address both the power and PNS concerns is to utilize a smaller gradient coil for head-only imaging (16, 17). Table 1 provides a summary of local head gradient coil designs. The earlier designs (18-26) demonstrated the potential for head gradient coils to achieve higher gradient performance. However these designs either lacked active shielding (18-22, 23, 24), or had a small (<22 cm) field-of-view (FOV) (18-22, 23-25), or had a small inner diameter (<40 cm) (18-27, 29) that might not accommodate the radiofrequency (RF)

transmit and phased-array assemblies used clinically today. Two designs at 7T had been reported (27-28), but with limited *in vivo* studies. Only one head gradient system (Siemens Allegra) had been widely available and it had an inner diameter of 36 cm and gradient performance of 40 mT/m gradient amplitude and 400 T/m/s slew rate.

In this work, we report on improvements to EPI distortion using a recently-developed, dedicated head gradient coil (referred to as the HG coil) at 3T (30). This HG coil incorporates active shielding, large FOV (26 cm) and a wide inner diameter (42 cm). It has maximum achievable gradient amplitude of 85 mT/m and 708 T/m/s slew rate (SR) when driven by standard clinical MRI system gradient drivers and power supplies. In standard clinical MRI systems, the gradient drivers generate an output of between 600-900A and 1600-2200V. Preliminary imaging studies using this HG coil demonstrated the feasibility for EPI acquisition at up to SR = 700T/m/s with minimal or no PNS (31).

METHODS

Theory of EPI distortion

The theory behind and effects of distortion due to the EPI readout are well-reported (3-4, 7-10). The essential equations used for creating the simulated results are briefly reviewed here for completeness, following the notation of Munger et al (7). For 2D EPI, the effects of distortion primarily manifest in the blipped phase-encoded (y) direction. For an original 2D image I, the pixels in the phase-encoding and frequency-encoding directions are labeled by indices m and n respectively. It can be shown that the distorted image, I' with M samples in the y direction may be expressed as a one-dimensional convolution between the distortion point-spread-function (PSF) K and I:

$$I'_{m',n} = \Sigma_{m=0}^{M-1} I_{m,n} K_{m,n;m'}. \quad (1)$$

The 1-D PSF, K may be defined as a function of the B_0 field, ΔB and the elapsed time relative to the echo time TE, τ for the k-th EPI readout in the y direction:

$$K_{m,n;m'} = \Sigma_{k=0}^{M-1} e^{2\pi i \left(\frac{k\left(m'-m\right)}{M} - \left(\frac{\gamma}{2\pi}\right)\Delta B_{m,n}\tau(k) \right)}. \quad (2)$$

For a single-shot, 2D EPI with a given ESP, τ is simply $k \times$ ESP, taking into account optimizations due to partial k-space sampling, rectangular field of view, and parallel imaging to reduce the total number of EPI readouts.

The mean pixel shift Δy in the phase-encoding direction depends on the B_0 homogeneity. Following the derivation in (3), it can be shown that for a y field-of-view (FOV_y) this pixel shift is given by

$$\Delta y_{m,n} = \frac{\gamma}{2\pi} ESP \times FOV_y \times \Delta B_{m,n} \quad (3)$$

with proportionate reduction when the echo train length is reduced using parallel imaging.

Head-gradient (HG) system

The HG coil used in this work has asymmetric transverse coils (X, Y-axes) and symmetric Z-axis coils. This coil had the following dimensions: outer diameter = 59 cm, length = 92 cm, and inner diameter = 42 cm. The HG coil was installed as an insert gradient coil in a conventional, wide-bore 3T scanner (MR750w, GE Healthcare, Waukesha, WI, USA), from which the body transmit/receive RF coil was removed. The whole-body gradient system was not removed physically, but was electrically-isolated by leaving the terminals open and insulated by electrical tape with 600V rating for safety. The mutual inductance between like-axes of the insert HG and the whole-body gradient coil was estimated to be an order of magnitude lower than the self-inductance of the insert coil, due to the actively-shielded design of the HG. This resulted in negligible image quality and safety issues during pulsing of the HG insert.

Standard clinical system electronics were connected to the HG, including the gradient driver which operated at peak current of 660 A and peak voltage of 1650 V with standard 25 kW of cooling. With this driver, the maximal gradient performance per axis was G_{max} = 85 mT/m and SR = 708 T/m/s. However, the system was operated typically with G_{max}=80 mT/m/s and SR=700 T/m/s. As compared to a whole-body gradient system, the compact and asymmetric HG design allowed for substantially increased PNS tolerance for simultaneous high G_{max} and high SR.

A sixteen-rung high-pass transmit/receive (T/R) RF birdcage coil was designed to be compatible with the HG coil, leaving a head-access bore diameter of 37 cm. An 8-dB attenuator was used in the transmit chain to reduce maximum RF power to 6 kW. For imaging studies, a 32-channel brain receiver array (Nova Medical, Wilmington, MA, USA) was used in conjunction with this birdcage transmit/receive coil. For patient-handling, the original bridge was removed and a short section of a similar bridge was installed on the patient-side end of the bore. This supported the patient's weight when the cradle was pushed from the docked table to the opening of the insert gradient coil.

Simulations of echo spacing against gradient performance

To characterize ESP as a function of improved gradient performance, two types of simulations were performed. First, EPI waveforms were first simulated to explore the parameter space using Matlab R2012b (Mathworks, Natick MA USA), keeping constant readout bandwidth (BW) of ± 250 kHz, and an imaging field-of-view (FOV) of 24 cm, suitable for brain imaging. The gradient performance was varied over the range of G_{max} = {10, 100} mT/m in steps of 1 mT/m and SR = {150, 700} T/m/s in steps of 10 T/m/s. The body and head PNS thresholds as reported in (16, 31) determined the safe operating points for the HG. Three in-plane sampling matrices were chosen: {80×80, 128×128, 192×192} for

{3, 1.9, 1.3} mm spatial resolution, respectively, with partial Fourier phase-encoding. The readout gradient amplitudes (G_R) tested were 23 mT/m (within whole-body PNS limits) and 46 mT/m (well above whole-body PNS limits, but close to head PNS limits). Ramp-sampling was applied in all cases to minimize ESP, whereby the area under the ramps were minimized (>10% of the total area) by taking advantage of the high SR.

The second simulation quantified the effects of ESP changes, spatial shift, and signal dropout due to EPI distortion at different slew rates. This was done to avoid confounding effects due to increased gradient non-linearity (32) and concomitant field effects (33) that might be associated with the asymmetric HG design. The SR was varied from 200 T/m/s to 700 T/m/s, keeping maximum readout gradient amplitude at 50 mT/m, which is the maximum gradient amplitude required for whole-brain EPI using a receiver bandwidth of ±250 kHz. The phase-encoding was assumed to be in the anterior-posterior direction with the readout in the left-right direction for axial scans. The 2D single-shot EPI acquisition was simulated with parameters of FOV = 24 cm, TR/TE = 5000/60 ms, 128×128 acquisition matrix, 3-mm slice thickness, and parallel imaging acceleration factor of 2 (R = 2). Spatial distortion and signal loss were simulated by applying Eqs. (1)-(2) to a T_2-weighted fast spin echo (FSE) reference acquisition. The simulated spatial shift (Δy) and the normalized signal level were measured in two (left and right) 1-cm^2 regions-of-interest (ROIs) located within each temporal lobe inferior to the Sylvian fissure (drawn by ETT). The standard deviations of the signal were determined based on the measurements in the selected ROIs.

To generate data for the simulation, informed consent was obtained from two healthy male subjects (ages = 32 and 42) for image acquisition under an IRB-approved protocol on a conventional 3T whole-body MRI system (MR750, GE Healthcare, Waukesha, WI, USA) with a peak gradient performance of G_{max} = 50 mT/m and SR = 200 T/m/s and a 32-channel brain coil (Nova Medical, Wilmington, MA, USA). The imaging protocol included an undistorted reference of an axial T_2- FSE scan (FOV = 24 cm, TR/TE = 10000/100 ms, 256×256 acquisition matrix, 3-mm slice thickness, 50 slices, partial Fourier factor = 0.75, parallel imaging using ASSET acceleration factor of R=2), and an axial 3D multi-echo gradient-echo acquisition with identical spatial sampling to obtain the B_0 field map (TR/TE = 50.0/3.1 ms, ΔTE = 3.3 ms, 14 echoes). For comparison against the simulation, single-shot spin-echo EPI was also acquired using the same simulated EPI parameters mentioned above.

In-vivo imaging with HG

Informed consent was obtained from five healthy male subjects (ages from 28 to 60) for MRI acquisition with the HG coil, under an institution review board (IRB)-approved protocol. Subjects were asked to report any sensation experienced during the course of the scan, with categories of ‘none’, ‘not painful’ and ‘painful’ for intensity and anatomical locations noted. Although the HG was capable of G_{max} = 85mT/m and SR = 708 T/m/s, for *in-vivo* imaging the performance was initially limited to a conservative G_{max} = 80 mT/m and SR = 500 T/m/s. The imaging protocol included spin-echo EPI acquisitions with parameters as mentioned in the previous section and at SR = {150, 200, 300, 500} T/m/s. Two sets of EPI images were acquired, one with phase-encoding direction anterior-posterior, and the other right-left. T_2 FSE and B_0 field map (TR/TE = 50.0/3.0 ms, ΔTE = 2.6ms, 16 echoes)

scans were also acquired to determine if there were either substantial image quality or B_0 differences compared to the whole-body gradient acquisitions. To exclude effects due to increased gradient nonlinearity of the HG coil, 3D gradient non-linearity correction (i.e. Gradwarp) with up to the tenth-order spherical harmonic correction (as compared to the fifth order used typically in whole-body scanner) was applied (34).

For analysis, two 1 cm^2 ROIs were also drawn (by ETT) in each temporal lobe on the images with SR = 150 T/m/s and anterior-posterior phase-encoding. For right-left phase-encoding, an ROI was selected for the right temporal lobe only to avoid selection of tissue-cerebrospinal fluid (CSF) boundary. The ROI signal was normalized to that of the SR = 500 T/m/s images. With N =15 (five subjects, 3 ROI each), a Wilcoxon rank-sum test was used to determine the significance, whereby $P < 0.05$ was considered significant.

The corresponding readout gradient amplitude obtained from the MR system from increasing SR = {150, 200, 300, 500} T/m/s were G_R = {23, 28, 35, 46} mT/m. With increased readout gradient, the concomitant field effects are expected to increase. However, the net effects on pixel shift are also subject to the reduced ESP as per Eq. (3). In this experiment, qualitative observations from the net effects from the concomitant field will be made.

To demonstrate the feasibility of clinical imaging at SR = 700 T/m/s, gradient-echo EPI was acquired on one subject using the HG coil at 1.5 mm-isotropic spatial resolution with no in-plane parallel imaging (FOV = 21 cm, 140×140 acquisition matrix, 1.5 mm slice thickness, TR/TE = 2000/31 ms, full-k_Y sampling, G_R = 54 mT/m, ESP = 376 μs, flip angle = 70°). The high slew rate allowed for a shorter TE (31 ms) to be achieved even without both parallel imaging (R = 1) and partial-Fourier sampling compared to a TE of 58 ms that may be achievable with a whole-body gradient. Such an acquisition is also suitable for fMRI studies. Diffusion-weighted EPI was also acquired using a two-shell diffusion acquisition with a total of 104 diffusion directions (12×b = 0 s/mm^2, 46×b = 1500 s/mm^2, 46×b = 3000 s/mm^2) also at 1.5 mm-isotropic spatial resolution with no in-plane parallel imaging (R = 1, FOV = 21 cm, 140×140 matrix, 93 slices at 1.5 mm slice thickness, TR/TE=3000/71 ms, partial Fourier factor = 0.75, G_R = 33.2 mT/m, ESP = 528 μs). With acceleration via simultaneous multislice (35) factor of 3, 31×3=93 slices were acquired in a total scan time of 5.2 minutes (104×3 s). In addition to regular T_2 (b=0), diffusion-weighted images, ADC and FA maps, kurtosis maps (36) were also computed. No EPI distortion correction (3, 7-11) was applied.

RESULTS

Simulations of EPI waveforms

Fig. 1 shows EPI gradient waveforms at various SR and sampling matrices. Whole-body PNS limits were imposed in Fig. 1a, but removed in Fig. 1b, resulting in shortening of ESP and the echo train duration by 19%. In Fig. 1c, the readout gradient amplitude was doubled from 23 mT/m to 46 mT/m, keeping within head PNS limits, resulting in a total of 48% reduction of both ESP and the echo train as compared to Fig. 1a. In Fig. 1d, the in-plane resolution was increased from 128×128 (parallel imaging acceleration factor R = 2) to

192×192 (R = 3), which increased ESP by 38%. In Fig. 1e, the PNS limits were not applied and readout gradient amplitude doubled, which reduced the ESP by 53%.

Fig. 2 summarizes the simulated waveform results, showing that ESP is more strongly influenced by SR than by G_{max} (Fig. 2a) when G_{max} is relatively large. As compared to commercially-available conventional whole-body MRI systems (G_{max} from 33 mT/m to 80 mT/m and SR ≤200T/m/s), the HG coil (SR = 700 T/m/s) is constrained by less restrictive head PNS limits. Fig. 2b-d show results of minimum achievable ESP vs. the readout gradient G_R at spatial resolutions of {3, 1.9, 1.3} mm. Increasing SR reduced the minimum ESP in each instance, although the benefits diminished with higher SR. These diminishing returns could also be observed in the increasing ESP contour intervals of Fig. 2a with increasing SR. Increased G_R also resulted in reduced ESP, with the exception of some instances of the lowest SR = 150 T/m/s and at 80×80 (Fig. 2b) and 128×128 (Fig. 2c) acquisition matrix, where the ESP minima of G_R ~ 30-35 mT/m occurred due to ramp-sampling. Increasing spatial resolution resulted in increased ESP, consistent with the results shown in the waveforms of Fig. 1.

Simulations of reduced distortion on brain images

Table 2 summarizes the results of ESP, spatial shift (Δy) and signal loss vs. the simulated SR, where the ESP reductions due to removal of PNS limits and increase in SR parallel those in Figs. 1-2. The improvement in Δy in the phase-encoding direction was approximately proportional to the reduction in ESP. There was also improvement in the intensity values (i.e. normalized mean values approach unity and standard deviation decrease) with reduced ESP, but their relationship was not a simple proportionality.

Fig. 3 compares the T2-FSE reference against the acquired EPI image and the simulated EPI-distorted images. As compared to the T2-FSE reference, the acquired SE-EPI image (Fig. 3a) had the familiar distortion effects of signal bunching or ‘pileup’ and signal dropout in the temporal lobe, as well as misalignment in the midbrain region and the occipital lobes. The effects of improved signal dropout and spatial shift shown in Table 2 are seen in the simulated images from Fig. 3b-d.

In-vivo imaging with HG – experimental verification

Out of five subjects scanned, one experienced sensation (on the face close to the bridge of the nose but below pain threshold) during EPI with frequency-encoding in the right-left direction (phase-encoding in anterior-posterior), and at the imaging SR of 500 T/m/s. No PNS was reported in the same subject when the frequency-encoding was selected to be in the anterior-posterior direction.

Fig. 4 compares the spin-echo EPI and B_0 field maps acquired on the whole-body system and the HG system in the same subjects. Image distortion and signal pile-up were visibly reduced in the HG results. We also noted that a slight reduction in ΔTE (from 3.3 to 2.6 ms) of the multi-echo gradient-echo scan used for B_0 mapping that was enabled by the high SR of HG.

In all *in-vivo* experimental scans, reduced signal dropout was observed as SR was increased from 150 T/m/s to 500 T/m/s. As compared to the SR = 500 T/m/s images, the lower SR images had increased signal dropout in the temporal lobes (both lobes for phase-encoding in anterior-posterior and only the right lobe for phase-encoding in right-left to avoid selection of CSF) by 7.5% (SR = 300 T/m/s, $P < 0.001$), 11.8% (SR = 200 T/m/s, $P < 0.001$), and 18.7% (SR = 150 T/m/s, $P < 0.001$). Fig. 5 shows images from one subject, demonstrating the improvements in EPI distortion from higher SR in either phase-encoding direction.

Fig. 6 provides an example of the combined effects of pixel shift resulting from changes in the concomitant field effect and reduced ESP. There was increased shift in the phase-encoding direction with the gradient amplitude of the EPI readout (G_R), resulting from the accumulated concomitant field that also affects ΔB that in turn affects Δy. However, a reduction in distortion was also observed with the reduced ESP resulting from the increased G_R. In addition, the extent of shift increased with the offset from iso-center in the superior direction.

Fig. 7 shows eight axial slices from the gradient-echo EPI acquisition at 1.5 mm-isotropic resolution with the HG coil operating at 80 mT/m and 700 T/m/s, showing relatively low spatial distortion and low signal dropout in the frontal and temporal lobes that are typically prone to EPI artifacts. Figure 8 shows axial slices as well as sagittal and coronal reformats of the diffusion scan at 1.5 mm-isotropic resolution, showing good whole-brain coverage, spatial linearity, and low spatial distortion effects.

DISCUSSION

In-vivo results of EPI with the dedicated head-only gradient system as installed in a conventional whole-body 3T magnet were presented. Imaging was performed at gradient amplitudes of 80 mT/m and slew rates of 500-700 T/m/s, which greatly exceeded whole-body systems specification. The EPI echo spacing obtained during imaging was substantially reduced (by approximately half), which agrees with predictions of gradient waveform simulations reported here. The improvements in distortion effects (reduced signal pile-up, dropout and shift) *in-vivo* were similar to those predicted in the simulation studies.

A preliminary demonstration of gradient-echo (for functional MRI) and diffusion EPI showed that low spatial distortion and signal dropout were feasible at 1.5 mm-isotropic spatial resolution, higher than that acquired conventionally with whole-body MRI (≥2 mm). In addition, with the reduction in TE times, an increase in image signal (due to T2 relaxation) was also realized, although this was not quantified in our study. Specifically, this demonstrates the potential for routine fMRI and diffusion scans with the head gradient without necessarily relying on in-plane parallel imaging. Note that increasing acceleration factors come at a cost to relative SNR, which is inversely proportional to $g\sqrt{R}$, where R is the acceleration factor and g is the coil geometric factor. This could mitigate SNR penalties associated with in-plane parallel imaging, which is typically needed in neuro MRI exams at 3T for reducing EPI distortion. Instead, parallel imaging could be applied with simultaneous multislice (35), which does not have an SNR penalty related to in-plane undersampling. With improved SNR, the slice thickness can be reduced, which improves slice resolution and

also reduces signal loss due to intravoxel dephasing for improving fMRI in the frontal and temporal lobe regions.

As compared to whole-body gradient designs, the HG design provides substantially increased gradient amplitude (peak of 85 mT/m) and maximum slew rate (708 T/m/s) with the same gradient driver power. This peak performance has been verified and tested previously in (31), which included detailed PNS threshold determination studies. Due to the HG coil's smaller size, increased G_{max} and SR could be applied simultaneously, which is not feasible with the whole-body gradient geometry. This expands the gradient waveform design space, which allows further optimization of the EPI waveform for better performance. In particular, the trade-off between ESP and readout gradient amplitude may be further explored. In addition, the reduced echo train duration may also permit reduced scan time (via reduction in repetition time) or increased multi-slice efficiency. The observation of reduced PNS in the anterior-posterior direction could be further exploited for pulse sequence optimization, as this was due to positioning of the anatomy that resulted in a much higher PNS threshold for the physical Y- and Z- directions (31).

There are drawbacks associated with the asymmetric HG design and its smaller form factor, but we believe that these can be partially or fully addressed. The increased extent of gradient nonlinearity for the equivalent head-sized imaging FOV required a higher order (e.g., 10^{th} order) 3D gradient nonlinearity correction as compared to the 5^{th} order correction used conventionally, and impacts the actual spatial resolution achieved. However, this resolution loss can be mitigated by improved approaches for gradient nonlinearity correction (37). In addition, both even and odd spherical harmonic terms were needed due to the asymmetric transverse gradient coil design. However, use of higher order terms did not add a substantial reconstruction time penalty.

The increased concomitant field effects, both from higher gradient amplitude and additional terms from the asymmetric design require additional correction schemes (38). For example, in EPI, this correction could involve changing gradient pre-emphasis and correction of the phase resulting from the concomitant field in image reconstruction; this topic is one focus area of our future work. In general, the concomitant gradient field is an additional field that is predictable given the known applied amplitudes of the gradient waveform. Asymmetric gradient coil designs also lead to asymmetric eddy current distribution in the conducting cylinders of the magnet, and the resulting high-order eddy current field disturbances may be more difficult to compensate. Further strategies for high-order eddy current correction include careful management of gradient-magnet interactions, as well as slice-dependent pre-emphasis (12-13) and post-processing correction, as demonstrated in (39).

The experiments with the HG were completed with a limited number of human subjects (five) with no known history of neurological disease. In addition, the results of 1.5 mm spatial resolution gradient-echo and diffusion-weighted spin-echo EPI were shown only in one subject.

The high SR capability benefits complementary approaches to improve EPI quality, such as image distortion correction (3,7-11), multi-shot EPI (6), and also 3D EPI. In addition, the

availability of increased gradient amplitude in the HG coil as compared to conventional whole-body gradients is expected to also benefit other gradient-intensive pulse sequences, such as phase-contrast velocimetry. The substantially reduced distortion seen in EPI due to the high SR should also benefit non-Cartesian readouts such as spirals, cones and shells. In this study, reduced echo time and inter-echo times were observed in the multi-echo gradient echo sequence, which might have reduced phase-aliasing in the B_0-maps. Gradient intensive readouts such as balanced steady-state free precession and fast spin echo may also benefit from reduced susceptibility to B_0 inhomogeneity and reduced blurring, respectively.

We have demonstrated improvements in EPI distortion in a dedicated head gradient coil capable of achieving high slew rates up to 700 T/m/s. The substantial reduction in EPI echo spacing can allow for higher spatial resolution to be achieved without substantial additional image distortion. This platform offers opportunities for advancement in diffusion imaging and functional MRI in terms of spatial resolution, geometric distortion, as well as increased image acquisition efficiency.

ACKNOWLEDGEMENTS

The authors will like to acknowledge useful discussion with John Schenck, Jean-Baptiste Mathieu, Peter Roemer and Christopher Hardy with regards to the motivation and system design and specification of the head gradient. The authors will also like to acknowledge useful discussion with Joshua Trzasko and Shengzhen Tao, with regards to image distortion and nonlinearity correction strategies, and with Andy Derbyshire with regards to EPI optimization. The authors also thank Matt Middione for help with reconstruction of simultaneous-slice-accelerated data, and Jonathan Sperl and Luca Marinelli for help with processing of diffusion data.

Grant support: NIH R01EB010065

REFERENCES

1. Mansfield P. Spatial mapping of the chemical shift in NMR. Magn Reson Med. 1984; 1:370–386. [PubMed: 6571566]
2. Kimmlingen R, Gebhardt M, Schuster J, Brand M, Schmitt F, Haase A. Gradient System Providing Continuously Variable Field Characteristics. Magn Reson Med. 2002; 47:800. [PubMed: 11948743]
3. Jezzard P, Balaban RS. Correction for geometric distortion in echo planar images from B0 field variations. Magn Reson Med. 1995; 34:65–73. [PubMed: 7674900]
4. Jezzard P, Clare S. Sources of distortion in functional MRI data. Human Brain Mapping. 1999; 8:80–85. [PubMed: 10524596]
5. Farzaneh F, Riederer SJ, Pelc NJ. Analysis of T2 limitations and off-resonance effects on spatial resolution and artifacts in echo-planar imaging. Magn Reson Med. 1990; 14:123–39. [PubMed: 2352469]
6. Pipe JG, Farthing VG, Forbes KP. Multishot diffusion-weighted FSE using PROPELLER MRI. Magnetic resonance in medicine. 2002; 47:42–52. [PubMed: 11754441]
7. Munger P, Crelier GR, Peters TM, Pike GB. An inverse problem approach to the correction of distortion in EPI images. IEEE Transactions on Medical Imaging. 2000; 19:681–9. [PubMed: 11055783]
8. Zeng H, Constable RT. Image distortion correction in EPI: comparison of field mapping with point spread function mapping. Magn Reson Med. 2002; 48:137–46. [PubMed: 12111941]
9. Andersson JLR, Skare S, Ashburner J. How to correct susceptibility distortions in spin-echo echo-planar images: application to diffusion tensor imaging. Neuroimage. 2003; 20:870–88. [PubMed: 14568458]

10. Morgan PS, Bowtell RW, Worthington BS. Correction of Spatial Distortion in EPI Due to Inhomogeneous Static Magnetic Fields Using the Reversed Gradient Method. J Magn Reson Imaging. 2004; 19:499–507. [PubMed: 15065175]
11. Holland D, Kuperman JM, Dale AM. Efficient correction of inhomogeneous static magnetic field-induced distortion in Echo Planar Imaging. Neuroimage. 2010; 50:175–83. [PubMed: 19944768]
12. Morrell G, Spielman D. Dynamic shimming for multi-slice magnetic resonance imaging. Magn Reson Med. 1997; 38:477–83. [PubMed: 9339449]
13. Lee S, Tan ET, Govenkar A, Hancu I. Dynamic slice-dependent shim and center frequency update in 3 T breast diffusion weighted imaging. Magn Reson Med. 2014; 71:1813–8. [PubMed: 23798360]
14. Han H, Song AW, Truong T. Integrated parallel reception, excitation, and shimming (iPRES). Magn Reson Med. 2013; 70:241–7. [PubMed: 23629974]
15. Stockmann JP, Witzel T, Keil B, Polimeni JR, Mareyam A, LaPierre C, Setsompop K, Wald LL. A 32-channel combined RF and B0 shim array for 3T brain imaging. Magn Reson Med 2015. doi: 10.1002/mrm.25587.
16. Chronik BA, Rutt BK. A comparison between human magnetostimulation thresholds in whole-body and head/neck gradient coils. Magn Reson Med. 2001; 46:386–394. [PubMed: 11477644]
17. Zhang B, Yen YF, Chronik BA, McKinnon GC, Schaefer DJ, Rutt BK. Peripheral nerve stimulation properties of head and body gradient coils of various sizes. Magn Reson Med. 2003; 50:50–58. [PubMed: 12815678]
18. Turner R, Jezzard P, Wen H, et al. Functional mapping of the human visual cortex at 4 and 1.5 tesla using deoxygenation contrast EPI. Magn Reson Med. 1993; 29:277–279. [PubMed: 8429797]
19. Wong, EC.; Hyde, JS. Perfusion imaging by interleaved excitation; Book of Abstracts: 10th Annual Scientific Meeting and Exhibition of the SMRM; San Francisco. 1991; abstract 791
20. Wong, EC.; Bandettini, PA.; Hyde, JS. Echo-planar imaging of the human brain using a three axis local gradient coil; Book of Abstracts: 11th Annual Scientific Meeting and Exhibition of the SMRM; Berlin. 1992; abstract 105
21. Abduljalil AM, Aletras AH, Robitaille PM. Torque free asymmetric gradient coils for echo planar imaging. Magn Reson Med. 1994; 31:450–453. [PubMed: 8208122]
22. Alsop DC, Connick TJ. Optimization of torque-balanced asymmetric head gradient coils. Magn Reson Med. 1996; 35:875–886. [PubMed: 8744016]
23. Crozier S, Doddrell DM. A simple design methodology for elliptical cross-section, transverse, asymmetric, head gradient coils for MRI. IEEE Trans Biomed Eng. 1998; 45:945–948. [PubMed: 9644905]
24. Bowtell R, Peters A. Analytic approach to the design of transverse gradient coils with co-axial return paths. Magn Reson Med. 1999; 41:600–608. [PubMed: 10204885]
25. Chronik BA, Alejski A, Rutt BK. Design and fabrication of a three-axis edge ROU head and neck gradient coil. Magn Reson Med. 2000; 44:955–963. [PubMed: 11108634]
26. Tomasi D, Xavier RF, Foerster B, Panepucci H, Tanns A, Vidoto EL. Asymmetrical Gradient Coil for Head Imaging. Magn Reson Med. 2002; 48:707. [PubMed: 12353289]
27. vom Endt, A.; Riegler, J.; Eberlein, E., et al. A High-Performance Head Gradient Coil for 7T Systems; Proceedings of the Joint Annual Meeting ISMRM-ESMRMB; Berlin. 2007; abstract 451
28. Green, D.; Pittard, S.; de Graaf, RA.; Nixon, TW.; Hetherington, HP. Asymmetric head gradient coil for imaging and spectroscopy at 7T; Proceedings of the 16th Annual Meeting of ISMRM; Toronto. 2008; abstract 346
29. Wade, TP.; Alejski, A.; Bartha, J., et al. Design, Construction and Initial Evaluation of a Folded Insertable Head Gradient Coil; Proceedings of the Joint Annual Meeting of ISMRM-ESMRMB; Milan. 2014; abstract 4851
30. Mathieu, J-B.; Lee, S-K.; Graziani, D., et al. Development of a Dedicated Asymmetric Head-only Gradient Coil for High-Performance Brain Imaging with a High PNS Threshold; Proceedings of the 23rd Annual Meeting of ISMRM; Toronto. 2015; abstract 1019
31. Lee S-K, Mathieu J-B, Graziani D, et al. Peripheral nerve stimulation characteristics of an asymmetric head-only gradient coil compatible with a high-channel-count receiver array. Magn Reson Med. (in press). doi: 10.1002/mrm.26044.

32. Tan, ET.; Lee, S-K.; Mathieu, J-B., et al. Gradient nonlinearity effects of diffusion weighted imaging in a dedicated head-only MRI system; Proceedings of the 21st Annual Meeting of ISMRM; Salt Lake City. 2013; abstract 3216

33. Meier C, Zwanger M, Feiweier T, Porter D. Concomitant field terms for asymmetric gradient coils: Consequences for diffusion, flow, and echo-planar imaging. Magn Reson Med. 2008; 60:128–134. [PubMed: 18581353]

34. Glover, GH.; Pelc, NJ. Method for correcting image distortion due to gradient nonuniformity. US Patent. 4,591,789. 1986.

35. Setsompop K, Gagoski BA, Polimeni JR, Witzel T, Van Wedeen J, Wald LL. Blipped-controlled aliasing in parallel imaging for simultaneous multislice echo planar imaging with reduced g-factor penalty. Magn Reson Med. 2011; 67:1210–24. [PubMed: 21858868]

36. Jensen JH, Helpern JA, Ramani A, Lu H, Kaczynski K. Diffusional kurtosis imaging: the quantification of non-gaussian water diffusion by means of magnetic resonance imaging. Magn Reson Med. 2005; 53:1432–40. [PubMed: 15906300]

37. Tao S, Trzasko JD, Shu Y, Huston J, Bernstein MA. Integrated Image Reconstruction and Gradient Nonlinearity Correction. Magn Reson Med. 2014; 74:1019. [PubMed: 25298258]

38. Tao, S.; Trzasko, JD.; Shu, Y.; Weavers, PT.; Lee, SK.; Bernstein, MA. Closed-Form Solution Concomitant Field Correction Method for Echo Planar Imaging on Head-only Asymmetric Gradient; Proceedings of the 23rd Annual Meeting of ISMRM; Toronto. 2015; abstract 3803

39. Xu D, Maier JK, King KF, et al. Prospective and retrospective high order eddy current mitigation for diffusion weighted echo planar imaging. Magn Reson Med. 2013; 70:1293–305. [PubMed: 23325564]

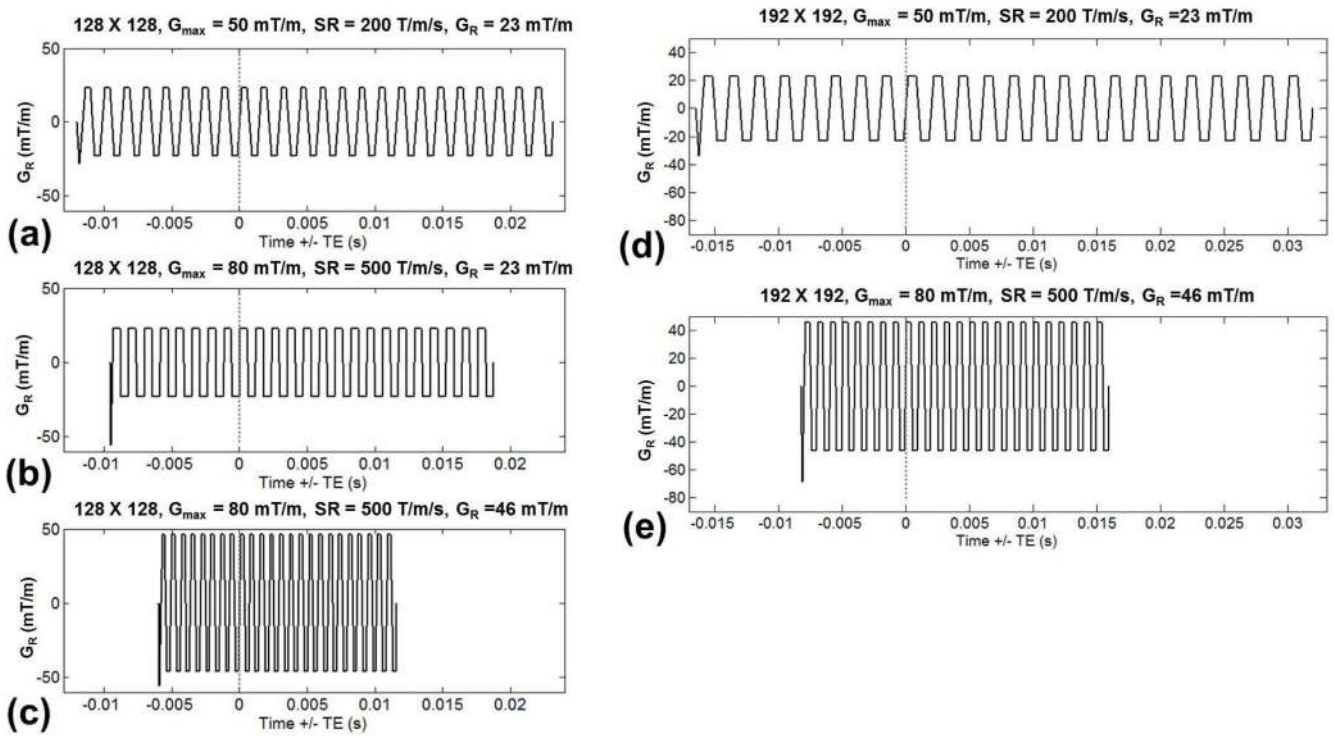

Figure 1.

Echo planar imaging (EPI) readout waveforms at different gradient amplitudes (G_{max}), slew rates (SR), applied readout gradient (G_R), and in-plane sampling matrix – (a-c) 128-by-128 with parallel imaging factor of 2 or (d-e) 192-by-192 with parallel imaging factor of 3. The waveforms are plotted relative to the echo time (TE), indicated by the dashed lines. As compared to EPI with a whole-body gradient (a), higher SR and removal of whole-body gradient PNS limits (b), along with increasing G_R (c), result in reductions of echo spacing and echo train length duration. These improvements are also seen at a higher in-plane sampling of 192-by-192 (from d to e).

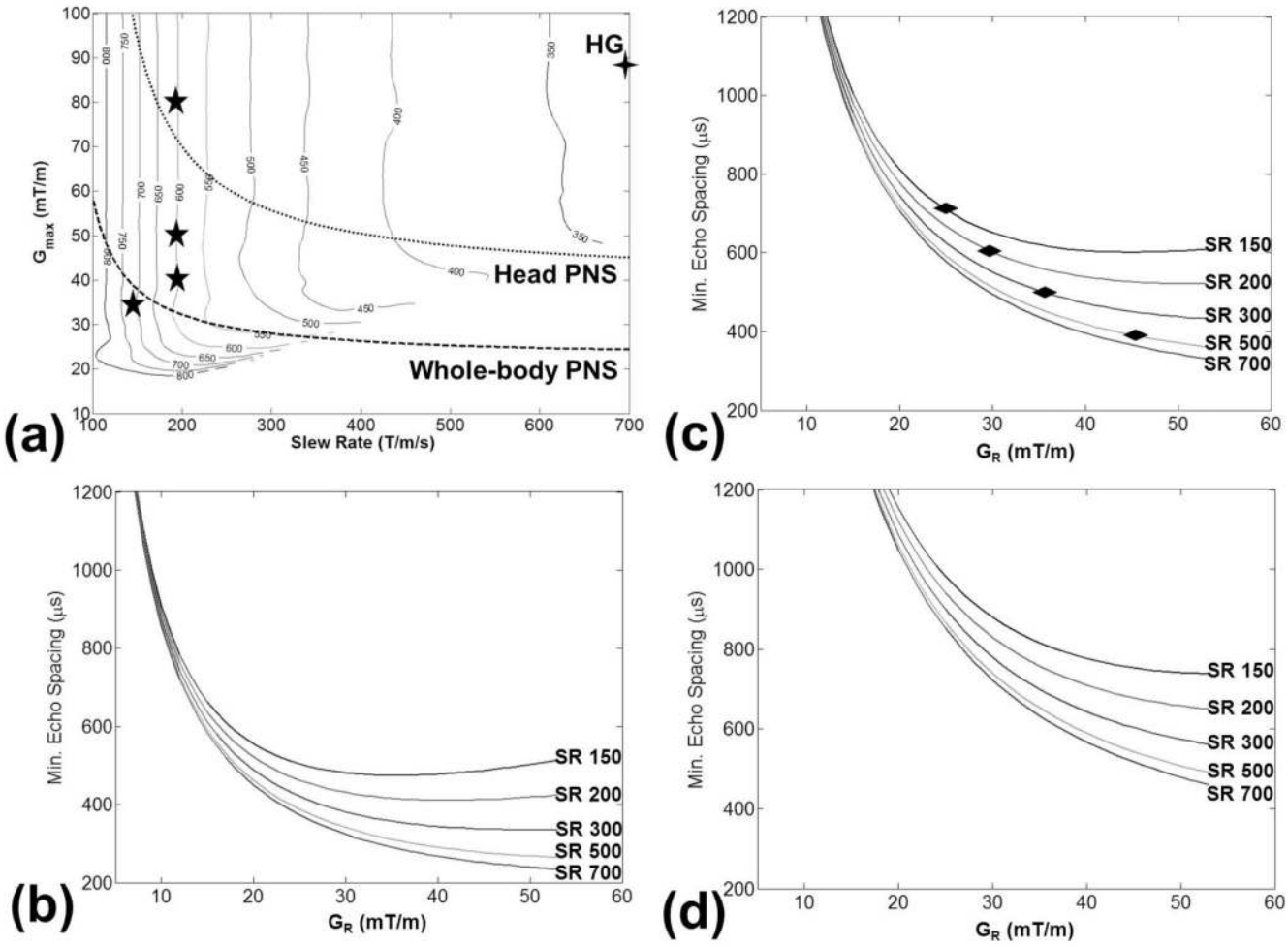

Figure 2.

EPI echo spacing (ESP) at various gradient performance levels (G_{max} and SR), and imaging parameters. (a) Contour plots of ESP (in μs) for an in-plane 128-by-128 sampling (FOV = 24 cm), where the five-pointed stars indicate peak performance levels of representative commercially-available whole-body MRI scanners, and the four-pointed star indicates peak performance of HG. PNS limit curves are based on Ref. (16), converting the peak-to-peak values to zero-to-peak values as shown here. Minimum ESP vs. readout gradient (G_R) for various SR (in T/m/s) at (b) 80-by-80, (c) 128-by-128, and (d) 192-by-192 acquisition matrix. Diamond marks in (c) indicate operating ESP and G_R for the *in-vivo* study.

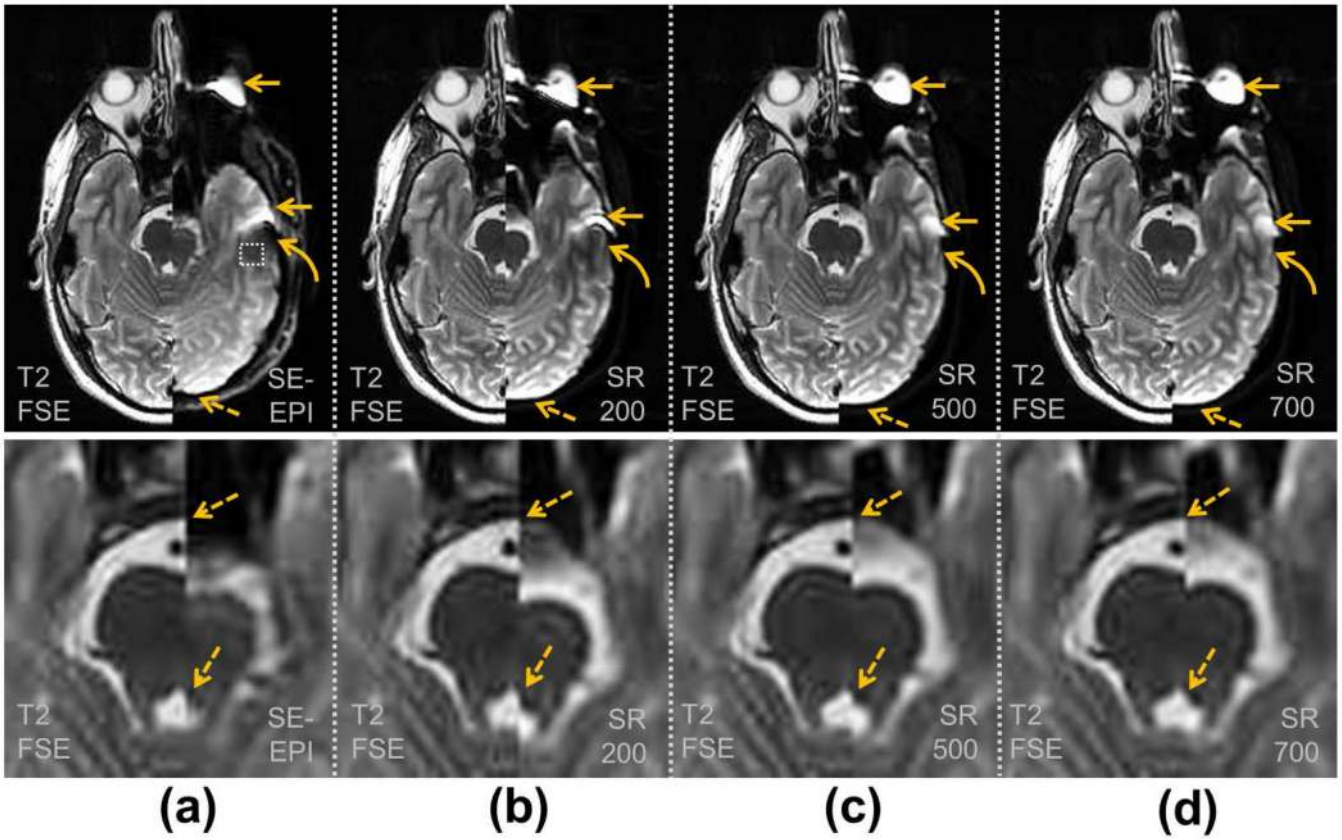

Figure 3.

Images of the T_2-FSE reference (left) and the spin-echo (SE)-EPI (right) in each column, displayed in a split screen. (a) T_2-FSE vs. the acquired SE-EPI (nominal SR = 200 T/m/s), (b) T_2-FSE vs. SR = 200 T/m/s, (c) T_2-FSE vs. SR = 500 T/m/s, (d) and T_2-FSE vs. SR = 700 T/m/s simulated images, showing reduced distortion effects. The dotted-edge box in (a) indicates an exemplary location of the ROI in the temporal lobe used in the analysis. The top row shows images at the full FOV, while the bottom row shows a magnified area in the midbrain region. The typical distortion effects of signal "pile-up" (arrow), signal dropout (curved arrow) and CSF boundary misalignment (dashed arrow) were progressively reduced with higher simulated SR.

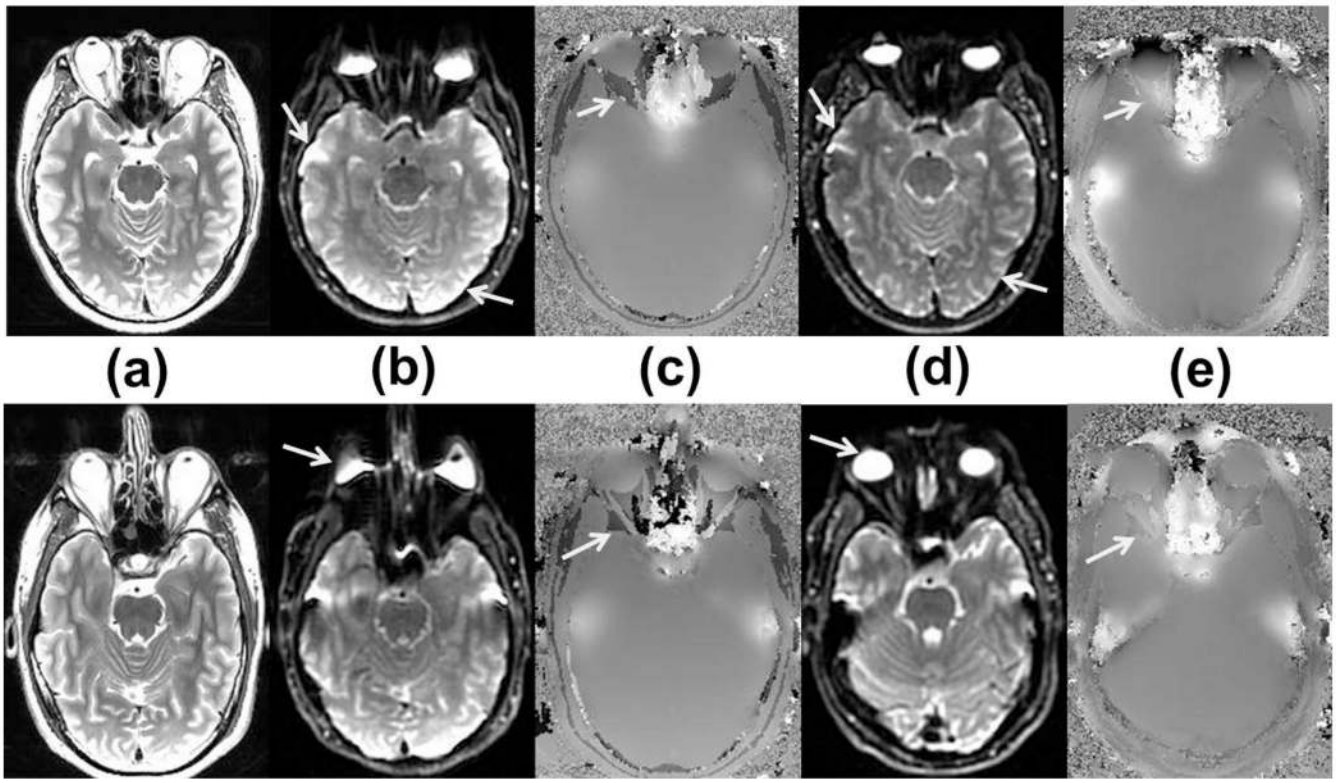

Figure 4.

Axial brain images from two human subjects (subject #4 top, #5 bottom rows) at approximately the same positions consisting of (a) whole-body gradient-acquired T_2-FSE, (b) whole-body spin-echo 2D EPI, (c) whole-body B_0 field map in the range of ±600 Hz, (d) a separately-acquired head-gradient spin-echo 2D EPI at SR = 500 T/m/s, and (e) head-gradient B_0 field map in the range of ±600Hz. The head-gradient images showed reduced signal 'pile-up' and improved intensity homogeneity (arrows in (b) and (d), top row), and reduced image distortion (arrows in (b) and (d), bottom row), in spite of increased non-uniformity of the B_0 map. Also, the reduced ΔTE of the head-gradient B_0 map seemed to provide reduced phase-aliasing (arrows in c, e).

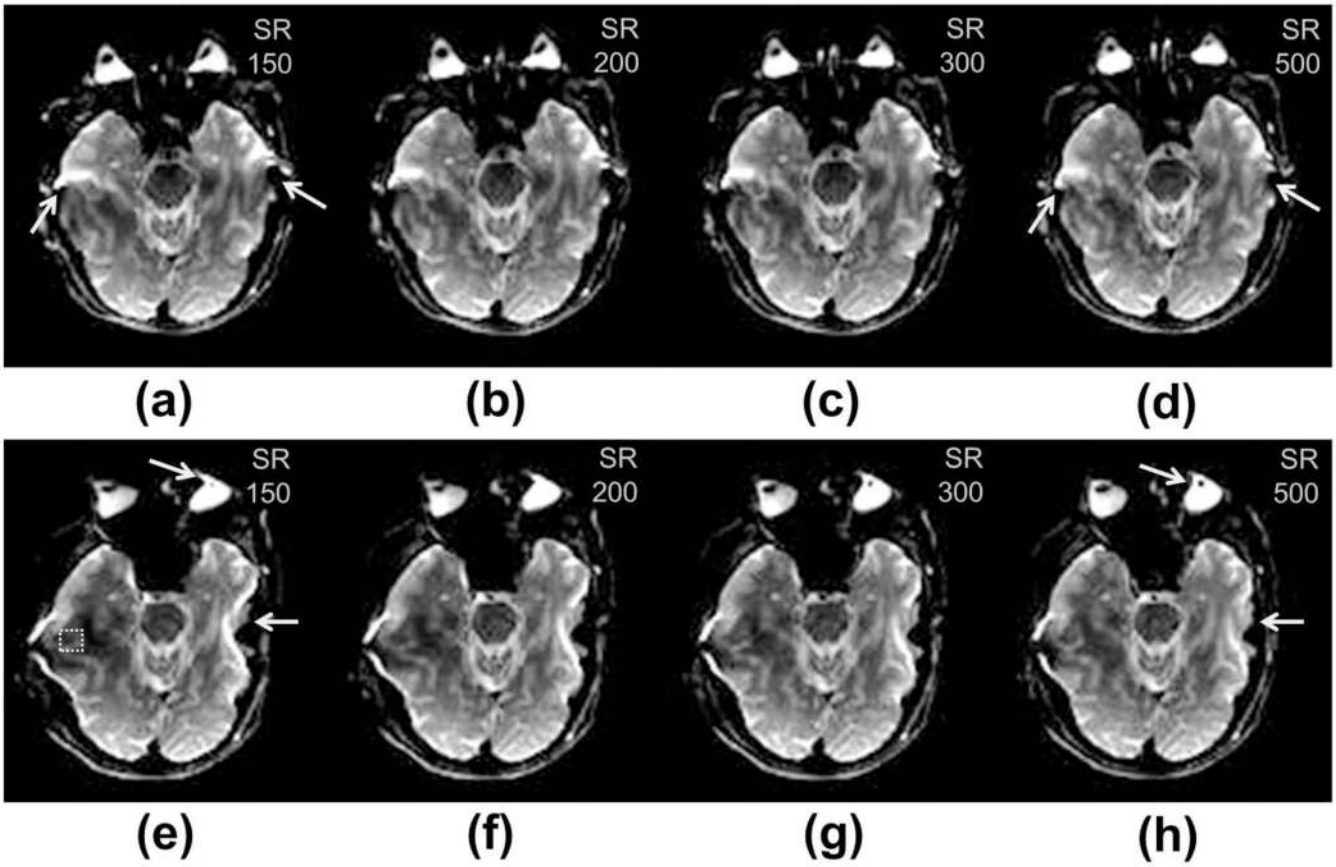

Figure 5.

Head-gradient, spin-echo 2D EPI images from a single subject (#1) acquired with phase-encoding along the (top row) anterior-posterior direction and (bottom row) right-left direction. Images were acquired at slew rates of (a, e) 150 T/m/s, (b, f) 200 T/m/s, (c, g) 300 T/m/s, and (d, h) 500 T/m/s. Progressive reduction in distortion effects within the temporal lobes was observed as slew rate was increased (arrows). The dashed square in (e) indicates an exemplary location of the ROI in the right temporal lobe used for analyzing signal dropout.

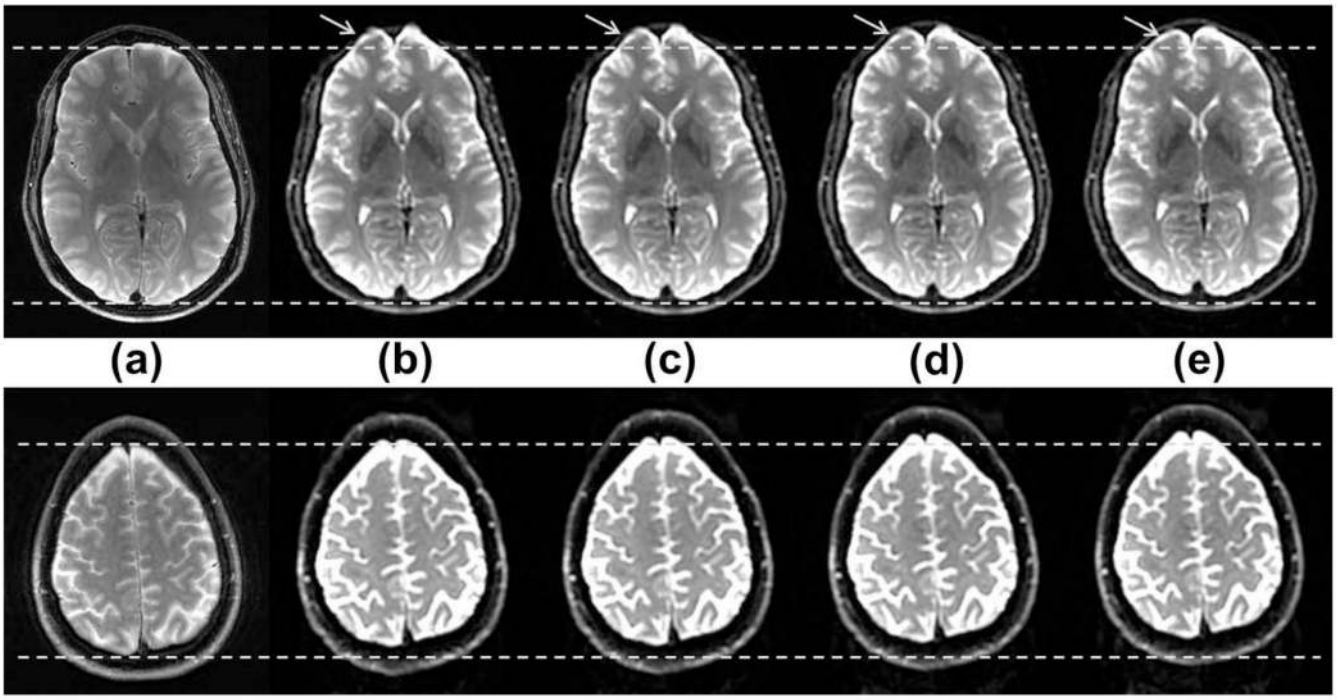

Figure 6.

Axial images mid-slice (top row) and 48 mm-superior slice (bottom row) from (a) T_2-FSE, and (b-e) 2D EPI with phase-encoding in the anterior-posterior (AP) direction and at applied readout gradients of (b) G_R = 23 mT/m and SR = 150 T/m/s, (c) G_R = 28 mT/m and SR = 200 T/m/s, (d) G_R = 35 mT/m and SR = 300 T/m/s and (e) G_R = 46 mT/m and SR = 500 T/m/s. With increased gradient slew rates, the readout gradient amplitude was also increased to optimize or maintain minimal ESP in the EPI acquisition. Increased offset in the AP direction was observed (comparing the horizontal dashed lines parallel to the AP extent of the brain) with increased G_R due to concomitant field effects. Improved distortion was also observed with increased G_R (arrows).The superior location (bottom row) had increased offsets compared to the mid-slice location (top row).

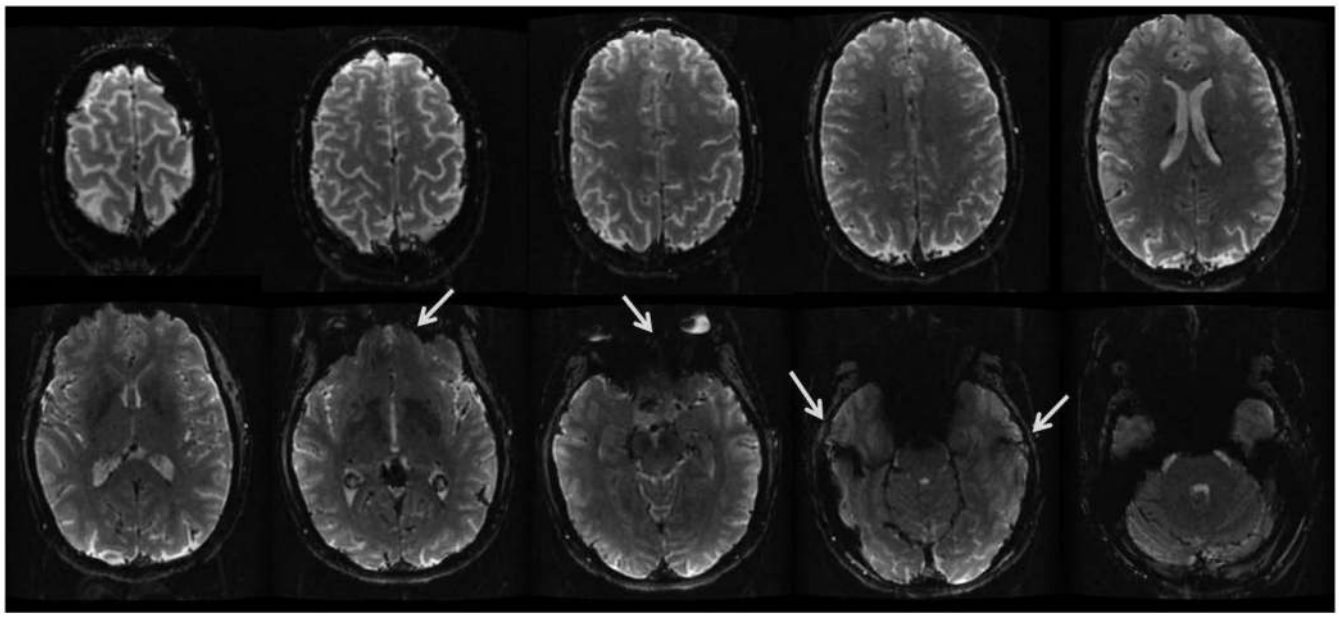

Figure 7.

Selected slices from a single-shot, 2D gradient-echo EPI acquired with the head gradient (G_{max} = 80mT/m, SR = 700T/m/s) at 1.5 mm-isotropic resolution with no in-plane parallel imaging, TE = 31 ms. Low spatial distortion was observed, along with minimal signal dropout in the frontal and temporal lobes (arrows) of the brain that are commonly seen in imaging with conventional whole-body MRI systems at 3T.

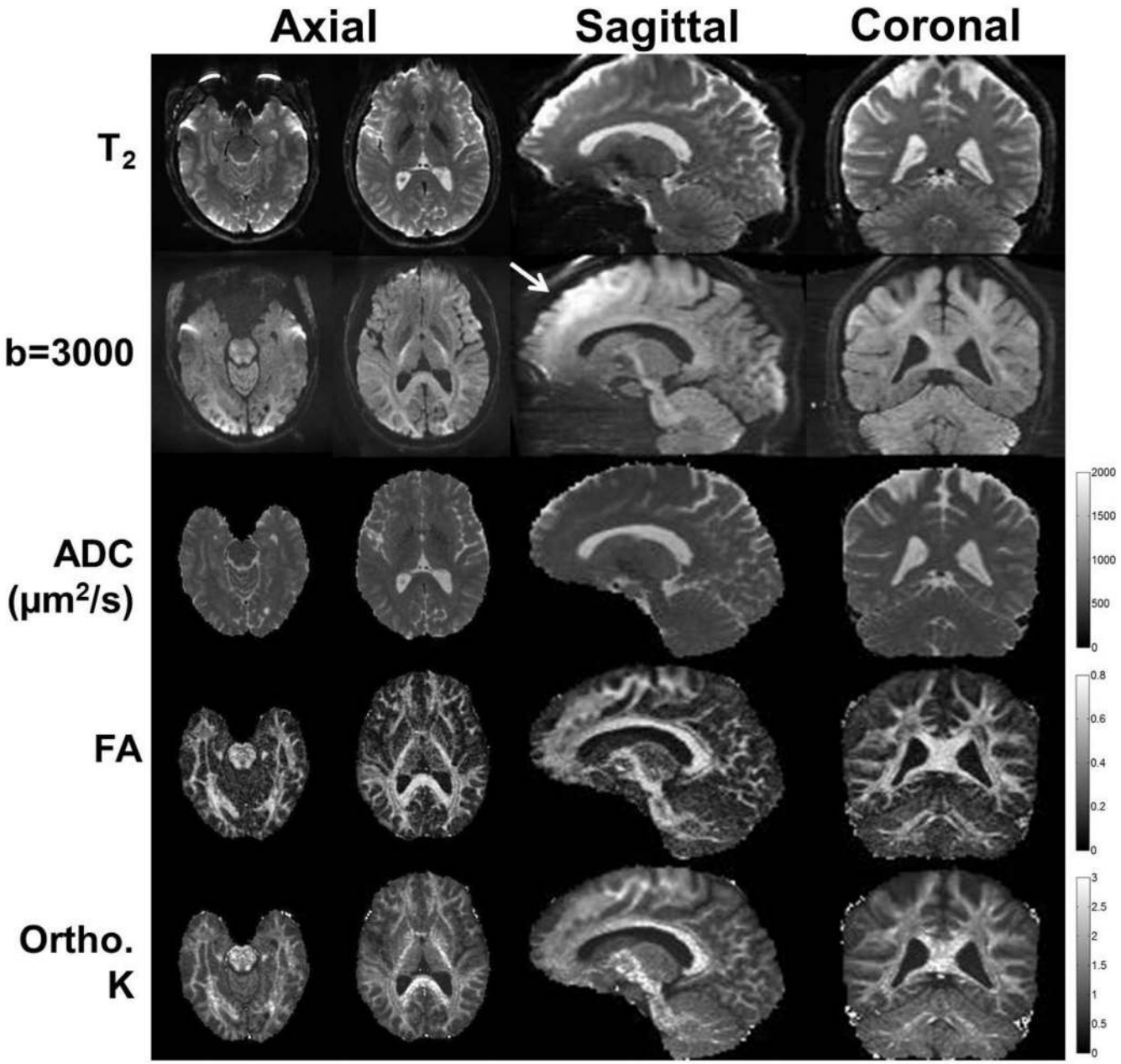

Figure 8.

Axial, multi-shell diffusion imaging at 1.5 mm-isotropic resolution with the HG coil (G_{max} = 80mT/m, SR = 700T/m/s) and corresponding sagittal and coronal plane reformats. The T_2 (b=0), b=3000 s/mm^2 diffusion images, apparent diffusion coefficient (ADC), fractional anisotropy (FA), and orthogonal kurtosis (K) maps are shown. Good linearity, whole-brain coverage, and low spatial distortion were observed. Hyperintensity was observed in the b=3000 s/mm^2 image due to uncorrected-for concomitant field effects (arrow).

Table 1

Summary of head gradient designs and specifications.

Ref./ Year	B_0 (T)	Active Shielding	Asymmetric transverse coils	Gradient coil outer diameter (cm)	Gradient coil inner diameter (cm)	FOV (cm)	Designed G_{max} (mT/m)*	Designed SR (T/m/s)*
18/1990	1.5	-	-	-	27	20	-,-,42.9	-
19/1991	1.5	-	-	-	10	-	80,80,210	1429
20/1992	1.5	-	-	-	30.5	-	20.3,21.1,21.7	362,377,387
21/1994	1.5	-	X	-	27.2-31.2	15^	16.3,13.2,22.3	136,110,279
22/1996	1.5	-	X	32	30	16^	50	200
23/1999	1.5	X	X	53	32	22#	32.7,31.8,32.7	130
24/1999	3	-	-	67.4	38.8	18^	19.9,20.5,75.6	140,160,230§
25/2000	1.5	-	-	42	32	12^	90,76,-	337,285,-
26/2002	0.5	X	X	-	33.6	-	-	-
@/2003	3	X	X	-	36	22#	40	400
27/2007	7	X	X	67	40	-	80	400
28/2008	7	X	X	67.5	42	24#	60§	481§
29/2014	3	X	-	47.2	34	17-22	80	2935
30/2015	3	X	X	59	42	26#	85	700

*3 comma-separated values: X, Y, Z axes. 1 value: individual axis.

^Approximation as summarized in Table 4 of Ref. (25) for 5% region of uniformity.

#Diameter of Spherical Volume (DSV) specified.

§Estimated based on known gradient driver capability and reported coil inductance.

@Siemens Allegra

Table 2

The tested gradient slew rates, the resulting EPI echo spacing (ESP), and simulation results of shifts in the phase-encoding direction, and normalized intensity changes in the right and left temporal lobes. With the exception of (*), whole-body PNS limits on gradient waveforms were disabled.

Slew Rate (T/m/s)	ESP (μs)	Right Temporal Lobe		Left Temporal Lobe	
		Mean/s.d. shift (mm)	Mean/s.d. intensity	Mean/s.d. shift (mm)	Mean/s.d. intensity
200*	724*	−5.7/3.2	0.76/0.14	−11.5/1.2	0.63/0.19
200	588	−4.6/2.7	0.82/0.13	−9.3/1.1	0.67/0.19
300	475	−3.7/2.2	0.88/0.12	−7.5/0.9	0.71/0.18
500	375	−2.8/1.7	0.93/0.10	−5.9/0.7	0.76/0.17
700	344	−2.6/1.6	0.95/0.09	−5.4/0.7	0.79/0.17